

# A Highly Reversible Room-Temperature Sodium Metal Anode

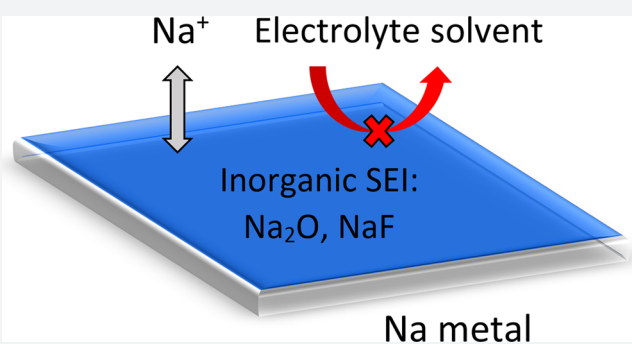
Zhi Wei Seh,<sup>†,‡</sup> Jie Sun,<sup>†</sup> Yongming Sun,<sup>†</sup> and Yi Cui<sup>\*,†,§</sup>

<sup>†</sup>Department of Materials Science and Engineering, Stanford University, Stanford, California 94305, United States

<sup>§</sup>Stanford Institute for Materials and Energy Sciences, SLAC National Accelerator Laboratory, Menlo Park, California 94025, United States

## S Supporting Information

**ABSTRACT:** Owing to its low cost and high natural abundance, sodium metal is among the most promising anode materials for energy storage technologies beyond lithium ion batteries. However, room-temperature sodium metal anodes suffer from poor reversibility during long-term plating and stripping, mainly due to formation of nonuniform solid electrolyte interphase as well as dendritic growth of sodium metal. Herein we report for the first time that a simple liquid electrolyte, sodium hexafluorophosphate in glymes (mono-, di-, and tetraglyme), can enable highly reversible and nondendritic plating–stripping of sodium metal anodes at room temperature. High average Coulombic efficiencies of 99.9% were achieved over 300 plating–stripping cycles at 0.5 mA cm<sup>-2</sup>. The long-term reversibility was found to arise from the formation of a uniform, inorganic solid electrolyte interphase made of sodium oxide and sodium fluoride, which is highly impermeable to electrolyte solvent and conducive to nondendritic growth. As a proof of concept, we also demonstrate a room-temperature sodium–sulfur battery using this class of electrolytes, paving the way for the development of next-generation, sodium-based energy storage technologies.



## INTRODUCTION

The need for high-energy, lightweight and low-cost rechargeable batteries has prompted the search for new battery technologies beyond conventional Li ion intercalation chemistry.<sup>1–14</sup> Rechargeable, room-temperature Na metal batteries, such as Na–S and Na–O<sub>2</sub>, are among the most promising candidates due to the low cost and high natural abundance of Na metal.<sup>15–22</sup> In contrast to widely studied Li ion and Na ion batteries, which are based on intercalation of Li<sup>+</sup>/Na<sup>+</sup> into layered anode materials,<sup>1–14</sup> Na metal batteries operate based on repeated plating and stripping of Na metal anodes, which possess a high theoretical specific capacity of 1166 mAh g<sup>-1</sup>.<sup>15–22</sup> This endows room-temperature Na–S and Na–O<sub>2</sub> batteries with high theoretical specific energies of 1274 and 1605 Wh kg<sup>-1</sup> respectively, which are 3 to 4 times that of existing Li ion batteries today (Figure S1).<sup>15–22</sup> Furthermore, room-temperature Na metal batteries are much safer compared to existing high-temperature, molten Na–S and Na–NiCl<sub>2</sub> batteries, hence making them suitable for both stationary grid storage and transportation applications.<sup>11</sup>

In the field of room-temperature Na metal batteries, notable progress has been made on the cathode side (e.g., S and O<sub>2</sub>),<sup>15–22</sup> but the crucial problems on the Na metal anode side remain largely unsolved. In particular, Na metal anodes are plagued with poor reversibility during repeated plating and stripping due to high reactivity with the electrolyte.<sup>4,5</sup> Based on decades of intensive research on Li metal anodes, it is widely believed that simple, additive-free liquid electrolytes are unable

to form a uniform and compact solid electrolyte interphase (SEI) to passivate alkali metal surfaces effectively.<sup>23–34</sup> This not only exposes fresh metal to react with the electrolyte solvent, leading to low Coulombic efficiency, but also promotes nonuniform ionic flux, leading to dendritic growth (Figure 1a). The growth of dendrites results in constant breaking and re-forming of the SEI, causing the battery to eventually fail due to depletion of electrolyte and high impedance through the thick SEI (Figure 1a). Moreover, dendrites can penetrate the separator and short-circuit the battery, posing serious safety hazards. An ideal electrolyte should be able to form a uniform and compact SEI on the Na metal surface, one which is highly impermeable to electrolyte solvent and conducive to nondendritic Na growth during long-term plating and stripping (Figure 1b). To date, there have only been a handful of reports exploring electrochemical plating and stripping of Na metal at room temperature, most of which use chloroaluminate ionic liquid electrolytes and only demonstrate 1 cycle with poor short-term reversibility (<97% Coulombic efficiency).<sup>35–40</sup> To the best of our knowledge, long-term reversibility of Na metal anodes remains a critical yet unexplored field.

Herein we report for the first time, that a simple liquid electrolyte, NaPF<sub>6</sub> (sodium hexafluorophosphate) in glymes (mono-, di-, and tetraglyme), can enable long-term, highly reversible and nondendritic plating–stripping of Na metal

Received: October 2, 2015

Published: November 2, 2015

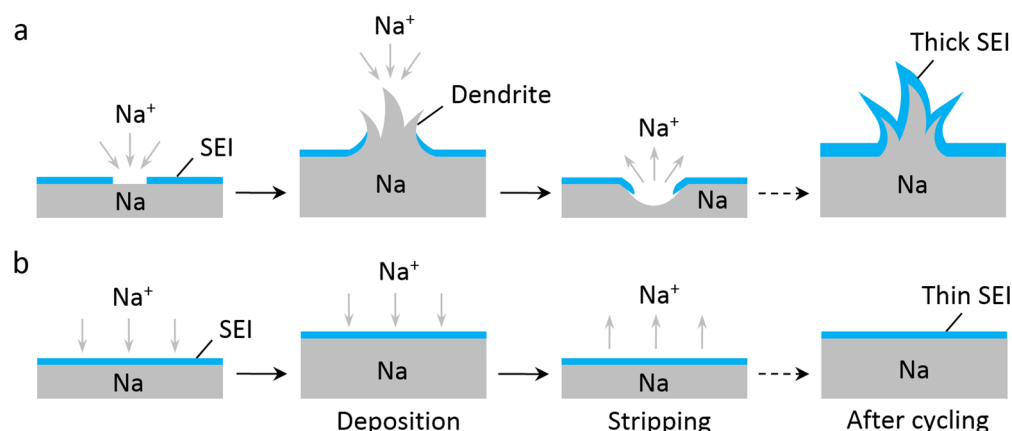


**Figure 1.** Schematics showing the difference between (a) dendritic and (b) nondendritic Na deposition.

anodes at room temperature. High average Coulombic efficiencies of 99.9% were achieved over 300 plating–stripping cycles at  $0.5 \text{ mA cm}^{-2}$ , without the use of any solid/polymer gel electrolyte, separator modification or anode surface coating. Both the electrolyte salt and solvent were found to be important in achieving this long-term reversibility. Further characterization revealed that  $\text{NaPF}_6$  in glymes formed uniform SEIs made of inorganic  $\text{Na}_2\text{O}$  and  $\text{NaF}$ , which are highly impermeable to electrolyte solvent and conducive to nondendritic growth.

## RESULTS AND DISCUSSION

To evaluate the reversibility of Na plating and stripping in various electrolytes, coin cells were assembled with Cu and Na as the working and counter electrodes, respectively. In each cycle, a fixed areal capacity ( $1 \text{ mAh cm}^{-2}$ ) of Na was deposited onto Cu foil at  $0.5 \text{ mA cm}^{-2}$ , which was then stripped by charging to  $1 \text{ V vs Na}^+/\text{Na}$ . The Coulombic efficiency for each cycle, which is a measure of the reversibility, was calculated based on the ratio of the capacity of Na stripped to that of Na deposited.<sup>27</sup> Using  $1 \text{ M NaPF}_6$  in diglyme as the electrolyte, a high average Coulombic efficiency of 99.9% was attained over 300 plating–stripping cycles (Figure 2a). This is the first demonstration of a Na metal anode with such long-term reversibility. The average voltage hysteresis between plating and stripping was also found to be small, ranging from 13.3 to 19.5 mV, indicating good kinetics (Figure 2b; see also Figure S2 for cyclic voltammograms). Examination of the Na metal surface revealed uniform and nondendritic morphologies after 1 cycle (Figure 2c,d), as well as after 300 cycles (Figure S3). Some regions of nodule-like Na deposits were also observed (Figure S4). Moreover, highly reversible plating–stripping of Na metal can be achieved using  $1 \text{ M NaPF}_6$  in monoglyme and tetraglyme, both of which exhibit average Coulombic efficiencies of 99.9% over 300 cycles as well (Figure 3a; see also Figure S5 for voltage profiles). The deposition morphologies were also found to be nondendritic in both cases (Figure S6).

In comparison, other electrolyte salt–solvent combinations were unable to achieve such high reversibility. Using  $\text{NaPF}_6$  in carbonate solvents, e.g.,  $1 \text{ M NaPF}_6$  in 1:1 v/v ethylene carbonate/diethyl carbonate (EC/DEC) and ethylene carbonate/dimethyl carbonate (EC/DMC), we found low Coulombic efficiencies that were less than 25% (Figure 3a). Using a different electrolyte salt in diglyme, e.g.,  $1 \text{ M NaN}(\text{SO}_2\text{CF}_3)_2$  (sodium bis(trifluoromethanesulfonyl)imide; NaTFSI),  $1 \text{ M}$

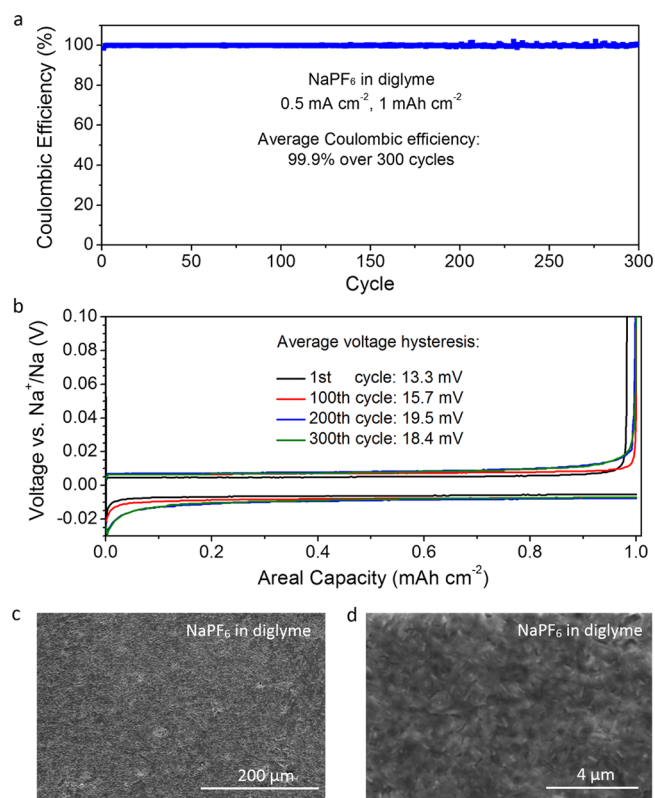


**Figure 2.** (a) Plating–stripping Coulombic efficiencies and (b) voltage profiles and average voltage hysteresis, as well as (c) low- and (d) high-magnification SEM images of Na metal anodes after 1 cycle, cycled at  $0.5 \text{ mA cm}^{-2}$  and  $1 \text{ mAh cm}^{-2}$  using  $1 \text{ M NaPF}_6$  in diglyme.

$\text{NaN}(\text{SO}_2\text{F})_2$  (sodium bis(fluorosulfonyl)imide; NaFSI),  $1 \text{ M NaSO}_3\text{CF}_3$  (sodium trifluoromethanesulfonate; NaOTf) and  $1 \text{ M NaClO}_4$  (sodium perchlorate) in diglyme, we see significant decrease in Coulombic efficiencies upon cycling (Figure 3b). Examination of the Na metal surface showed nonuniform and/or dendritic deposition morphologies in all of these cases (Figure 3c–f and Figure S7).

Since the reversibility of Na metal anodes is largely dependent on the composition of the SEI,<sup>4,5</sup> we carried out X-ray photoelectron spectroscopy (XPS) with depth profiling to examine the SEI formed in these various electrolytes. To do so, the Na/Cu cells were disassembled in the stripped state after 10 plating–stripping cycles to examine the SEI remaining on

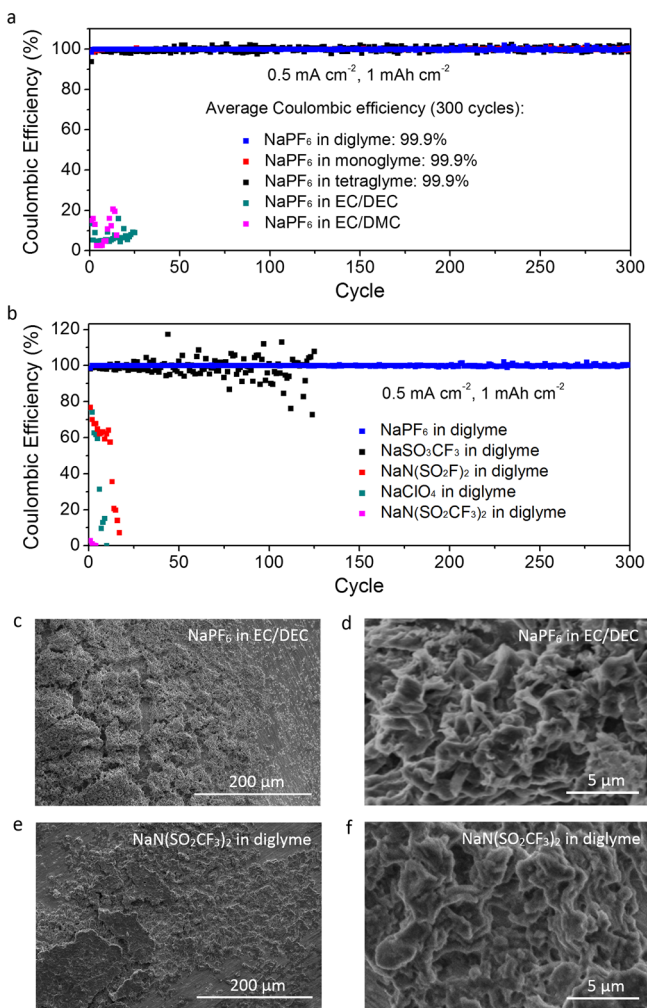


**Figure 3.** (a, b) Plating–stripping Coulombic efficiencies of Na metal anodes cycled using (a) 1 M NaPF<sub>6</sub> in various electrolyte solvents and (b) 1 M of various electrolyte salts in diglyme. (c–f) Low- and high-magnification SEM images of the Na metal surface after 1 cycle at 0.5 mA cm<sup>-2</sup> and 1 mAh cm<sup>-2</sup> using (c, d) 1 M NaPF<sub>6</sub> in 1:1 v/v EC/DEC and (e, f) 1 M NaN(SO<sub>2</sub>CF<sub>3</sub>)<sub>2</sub> in diglyme.

the Cu foil. To avoid exposure to air, the samples were transferred into the XPS chamber using a sealed Ar-filled vessel. First, we analyze the composition of the SEI formed using NaPF<sub>6</sub> in diglyme (Figure 4, Figures S8 and S9, and Table S1). At 0 min sputtering (Figure 4a), the C 1s spectrum can be fitted using 2 peaks with binding energies of 288.2 eV (C–O) and 284.8 eV (C–C, C–H), while the O 1s spectrum shows a corresponding peak at 535.5 eV (C–O), both of which are consistent with sodium alkoxides (RCH<sub>2</sub>ONa) being the main reduction product of diglyme.<sup>5–7</sup> The O 1s spectrum also shows a peak at 530.9 eV (Na–O) while the F 1s spectrum shows a peak at 683.8 eV (Na–F). Combining these analyses with the Na 1s spectrum, we deduce that the Na 1s feature at 1071.0 eV consists of 2 overlapping peaks (Na–O and Na–F), which are consistent with tabulated values for Na<sub>2</sub>O and NaF (Table S1).<sup>5–7</sup> These results indicate the formation of Na<sub>2</sub>O as the reaction product of Na metal with trace amounts of O<sub>2</sub> in the Ar-filled glovebox (<0.5 ppm), and NaF as the main reduction product of NaPF<sub>6</sub>. We note that the F 1s peak at 686.4 eV (P–F) occurs due to residual Na<sub>x</sub>PF<sub>y</sub> and Na<sub>x</sub>PO<sub>z</sub>F<sub>w</sub> species on the SEI surface (Figure 4a and Figure S8).<sup>5–7</sup>

Overall, we see that the top surface of the SEI contained both organic (RCH<sub>2</sub>ONa) and inorganic (Na<sub>2</sub>O, NaF) components.

After 1 min of sputtering to remove the top surface, the C and O peaks corresponding to organic RCH<sub>2</sub>ONa species became weak and indistinct (Figure 4b). Further sputtering up to 2, 3, and 8 min yielded the same result (Figure 4c–e). On the other hand, after 1 min of sputtering, the O, Na, and F peaks corresponding to inorganic Na<sub>2</sub>O and NaF remained strong and distinct (Figure 4b). This trend continued after 2 and 3 min of sputtering, after which the Na<sub>2</sub>O and NaF peaks became difficult to resolve (Figure 4c–e). Overall, these results indicate that the interior of the SEI consists largely of inorganic Na<sub>2</sub>O and NaF species, with very little organic reduction products present (Figure 5a). This tells us that NaPF<sub>6</sub> is capable of forming a uniform and compact SEI of Na<sub>2</sub>O and NaF which is highly impermeable to the electrolyte solvent. The uniformity of the SEI also promotes uniform Na<sup>+</sup> flux and nondendritic growth of Na metal, so that the SEI remains intact and stable during cycling. As a result, the SEI was found to be thin (~4 nm; Figure S9), leading to low and almost-constant charge transfer resistance during cycling, as evidenced by impedance spectroscopy (Figure 5b). Moreover, inorganic Na<sub>2</sub>O and NaF possess high shear moduli of 49.7 and 31.4 GPa respectively, which are 10 to 15 times that of Na metal (3.3 GPa; Table S2), making them capable of suppressing dendritic growth of Na metal, if any.<sup>25</sup> XPS analysis of the SEIs formed using NaPF<sub>6</sub> in monoglyme and tetraglyme showed similar results (Figure S10–S13 and Tables S3 and S4).

For comparison, we analyze the composition of the SEI formed using a different electrolyte salt, e.g., NaN(SO<sub>2</sub>CF<sub>3</sub>)<sub>2</sub> in diglyme (Figures S14 and S15 and Table S5). At 0 min of sputtering, we see both organic reduction products (RCH<sub>2</sub>ONa) and inorganic products (Na<sub>2</sub>O, NaF) on the top surface of the SEI as well (Figure S14a), similar to the case of NaPF<sub>6</sub> in diglyme. After 1 min of sputtering, all the peaks corresponding to RCH<sub>2</sub>ONa, Na<sub>2</sub>O, and NaF species still remained strong and distinct (Figure S14b). This trend persisted after 2, 3, and even 8 min of sputtering (Figure S14c–e), which indicates that, overall, the SEI contains both organic and inorganic products. This tells us that, although both NaPF<sub>6</sub> and NaN(SO<sub>2</sub>CF<sub>3</sub>)<sub>2</sub> form SEIs made of Na<sub>2</sub>O and NaF, the one formed by NaN(SO<sub>2</sub>CF<sub>3</sub>)<sub>2</sub> is less uniform and compact in nature. This causes more Na to be exposed to undesirable side reactions with the electrolyte solvent, forming more organic reduction products in the SEI and lowering the Coulombic efficiency. The presence of organic products, which are generally porous in nature, makes the SEI even more permeable to the electrolyte solvent upon cycling.<sup>5–7</sup> Moreover, the nonuniformity of the SEI results in nonuniform Na<sup>+</sup> flux and dendritic growth of Na metal, causing constant breaking and re-forming of the SEI. Therefore, the SEI was found to be much thicker (~22 nm; Figure S15), leading to much higher charge transfer resistance, which increases further upon cycling (Figure 5c). XPS analysis of the SEIs formed using the other electrolyte salts, NaN(SO<sub>2</sub>F)<sub>2</sub>, NaSO<sub>2</sub>CF<sub>3</sub>, and NaClO<sub>4</sub>, in diglyme showed similar results (Figures S16–S21 and Tables S6–S8). One possible explanation is that NaPF<sub>6</sub> might have a higher reduction potential than that of glyme solvents, leading to preferential reduction of NaPF<sub>6</sub> to form a uniform, inorganic SEI which protects the Na metal surface from subsequent reaction with the electrolyte solvent. In contrast, the other electrolyte salts could have reduction potentials that are comparable to or lower than those of glyme

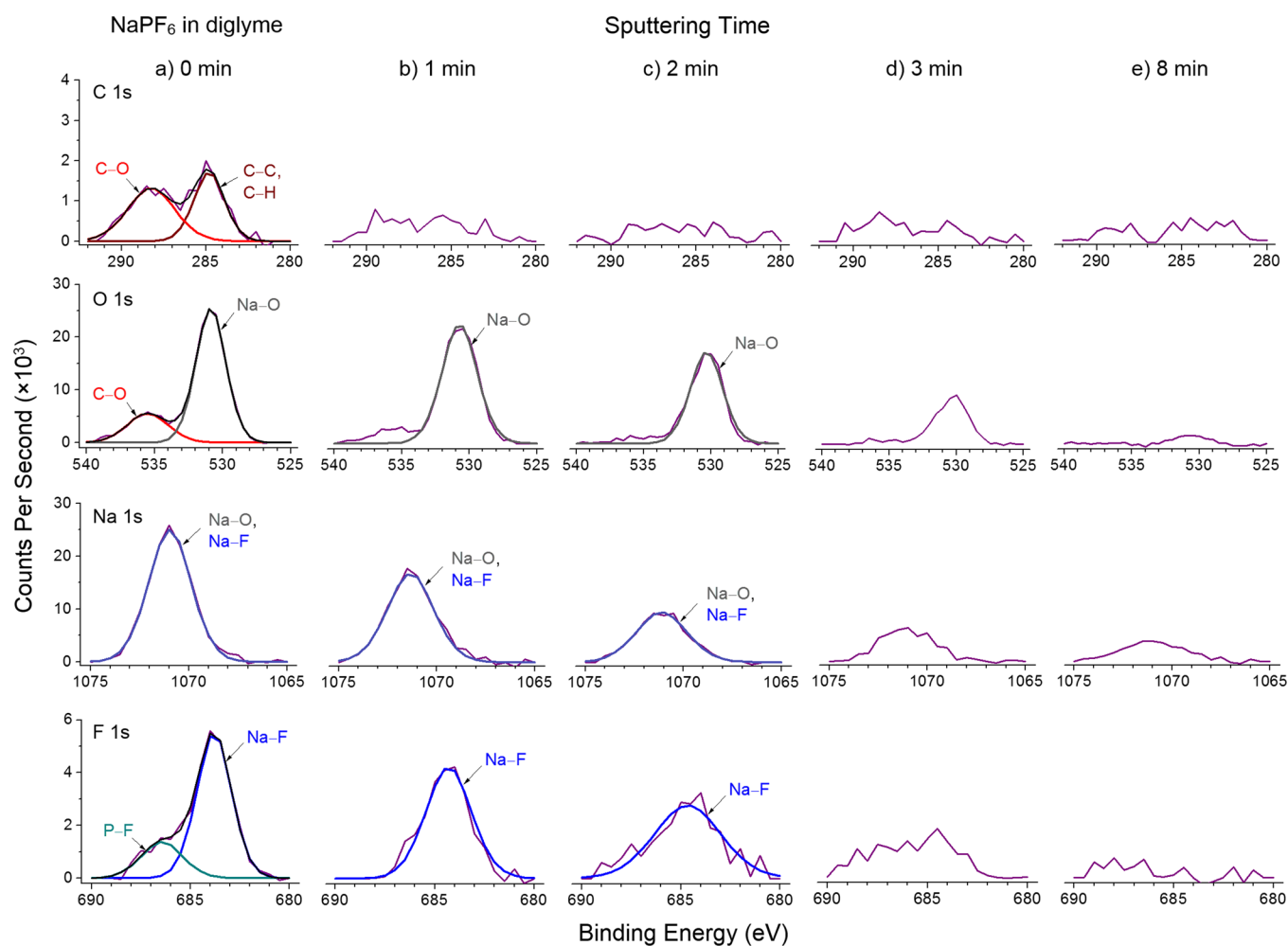


**Figure 4.** XPS characterization of the SEI formed using 1 M NaPF<sub>6</sub> in diglyme. The C 1s, O 1s, Na 1s, and F 1s spectra are displayed in rows, with corresponding depth profiling results in columns after (a) 0 min, (b) 1 min, (c) 2 min, (d) 3 min, and (e) 8 min of sputtering.

solvents, resulting in reduction of both the electrolyte salt and solvent to form a mixed organic–inorganic SEI.

In the case of NaPF<sub>6</sub> in carbonate solvents, e.g., NaPF<sub>6</sub> in EC/DEC and EC/DMC, we see strong and distinct XPS peaks corresponding to both organic reduction products (sodium alkyl carbonates; RCH<sub>2</sub>OCO<sub>2</sub>Na) and inorganic products (Na<sub>2</sub>O, NaF) on the top surface of the SEI (Figures S22–S25).<sup>5–7</sup> All the above peaks persisted even after 1, 2, 3, and 8 min of sputtering, which indicates that the SEI is made up of both organic and inorganic products (Figures S22–S25). This is because carbonate solvents are known to have higher reduction potentials and are more easily reduced on the Na metal surface compared to glymes, which leads to more undesirable organic components in the SEI.<sup>28</sup> As described earlier, a mixed organic–inorganic SEI would be more permeable to electrolyte solvent and prone to Na dendrite growth upon cycling, thus resulting in the formation of a thicker and more resistive SEI as observed (Figure Sd, Figures S23 and S25, and Tables S9 and S10).

The room-temperature ionic conductivities of NaPF<sub>6</sub> in mono-, di-, and tetraglyme were measured to be 10.8, 5.8, and 2.6 mS cm<sup>-1</sup> respectively, which is in line with the increasing viscosity of the solvents.<sup>41–43</sup> To evaluate the rate capability of the Na metal anodes, we cycled them using NaPF<sub>6</sub> in diglyme at increasing current densities, while keeping the areal capacity constant at 1 mAh cm<sup>-2</sup>. At high current densities of 1, 2, 3,

and 4 mA cm<sup>-2</sup>, average Coulombic efficiencies of 99.9%, 99.6%, 99.5%, and 99.2% could be attained respectively (Figure 6a). To demonstrate their reversibility for high-capacity applications, we also cycled them at increasing areal capacities while keeping the current density constant at 1 mA cm<sup>-2</sup>. At areal capacities of 1, 2, 4, 8, and 10 mAh cm<sup>-2</sup>, we demonstrate high average Coulombic efficiencies of 99.8%, 99.9%, 100.0%, 99.9%, and 100.0% respectively (Figure 6b). The Na deposition morphologies after cycling at increasing current densities and increasing areal capacities were found to be uniform and nondendritic as well (Figure S26; see also Figure S27 for voltage profiles). The electrochemical stability of NaPF<sub>6</sub> in mono-, di-, and tetraglyme was also studied, and the onset oxidation potentials were determined to be ~4.4, 4.5, and 4.7 V vs Na<sup>+</sup>/Na respectively (Figure S28), which is consistent with prior work.<sup>41–43</sup> This makes them suitable for use in a range of room-temperature Na metal batteries, including Na–S and Na–O<sub>2</sub>.<sup>15–22</sup> As a proof of concept, we demonstrate a room-temperature Na–S battery using NaPF<sub>6</sub> in tetraglyme as the electrolyte, which exhibited high specific capacity of 776 mAh g<sup>-1</sup><sub>S</sub> and good cycling stability (Figure 6c; see also Figures S29–S31 and Materials and Methods for details). Cyclic voltammograms showed cathodic peaks at 2.25 and 1.65 V which are attributed to the reduction of S<sub>8</sub> to long-chain sodium polysulfides (Na<sub>2</sub>S<sub>*n*</sub>, *n* = 4 to 8) and further reduction to short-chain sodium polysulfides (Na<sub>2</sub>S<sub>*n*</sub>, *n* = 1 to 3) respectively

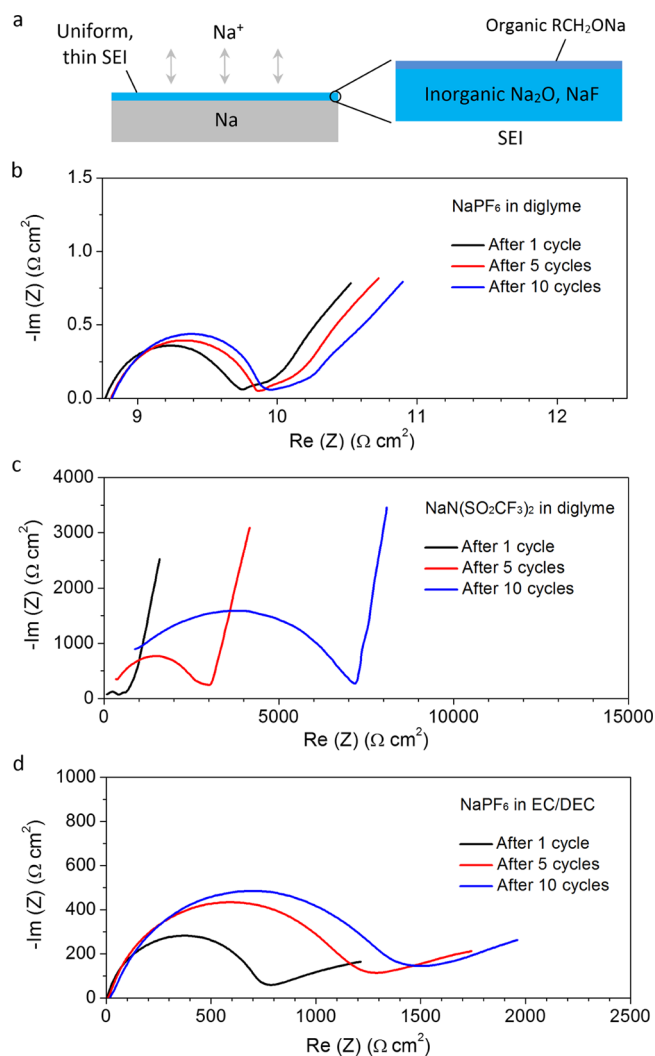


**Figure 5.** (a) Schematic showing the SEI formed on the Na metal surface using NaPF<sub>6</sub> in glymes. (b–d) Impedance spectra of Na metal anodes cycled using (b) 1 M NaPF<sub>6</sub> in diglyme, (c) 1 M NaN(SO<sub>2</sub>CF<sub>3</sub>)<sub>2</sub> in diglyme, and (d) 1 M NaPF<sub>6</sub> in 1:1 v/v EC/DEC.

(Figure S29).<sup>19</sup> Similarly, the anodic peaks at 1.85 and 2.40 V arise from the oxidation of short-chain polysulfides to long-chain polysulfides and further oxidation to S<sub>8</sub> respectively (Figure S29).<sup>19</sup> For comparison, Na–S batteries were also cycled using NaN(SO<sub>2</sub>CF<sub>3</sub>)<sub>2</sub> in tetraglyme, which showed faster capacity decay under identical testing conditions (Figure 6c). The use of NaPF<sub>6</sub> in EC/DEC as the electrolyte resulted in very low capacity after the first cycle due to irreversible reaction between long-chain polysulfides and carbonate solvents (Figure 6c).<sup>44–48</sup>

Although NaPF<sub>6</sub> of the highest commercially available purity was used (99+%), there was still a small amount of insoluble impurity in the as prepared electrolytes, which was determined to be NaF in previous work.<sup>42</sup> For comparison, we have also prepared electrolytes of NaPF<sub>6</sub> in diglyme, allowed the impurity to settle down, and extracted the supernatant for use in cycling of Na metal anodes. In the case without NaF impurity, the average Coulombic efficiency for Na plating and stripping over the first 100 cycles was found to be 99.9% as well (Figure S32). However, the average value dropped to 99.7% and 99.5% over the next 200 and 300 cycles respectively (Figure S32),

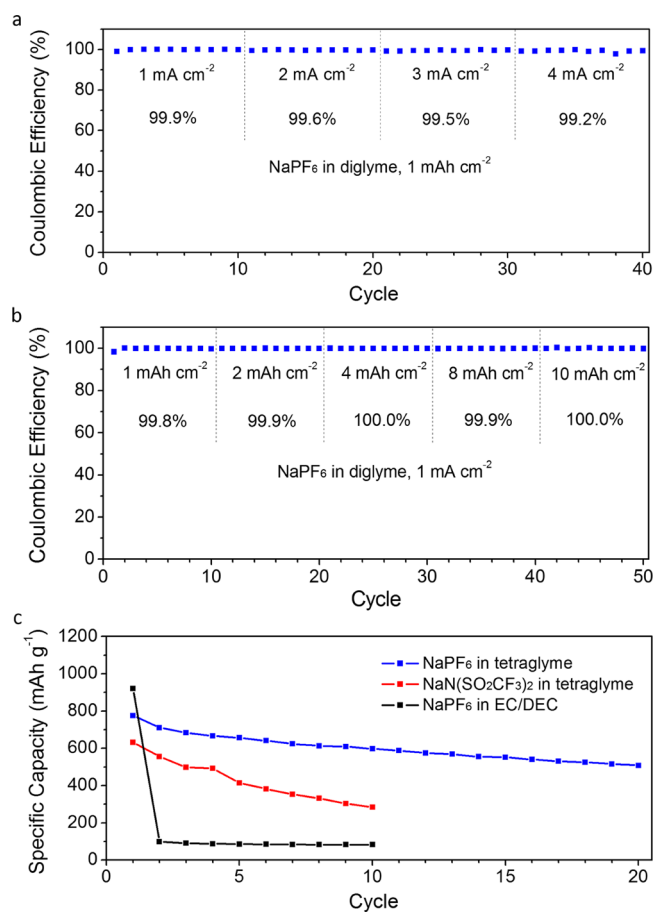


**Figure 6.** (a, b) Plating–stripping Coulombic efficiencies of Na metal anodes cycled using 1 M NaPF<sub>6</sub> in diglyme at (a) 1 mA cm<sup>-2</sup> with increasing current densities and (b) 1 mA cm<sup>-2</sup> with increasing areal capacities. (c) Specific capacities (calculated based on the mass of S) of room-temperature Na–S batteries cycled using various electrolytes at 0.1 C (1 C = 1673 mA g<sup>-1</sup>) from 1.2 to 2.8 V vs Na<sup>+</sup>/Na.

indicating that the small amount of NaF impurity has a stabilizing effect on the Na metal surface.

In conclusion, we report for the first time that a simple liquid electrolyte, NaPF<sub>6</sub> in glymes (mono-, di- and tetraglyme), can enable highly reversible and nondendritic plating–stripping of Na metal anodes at room temperature, without the use of any solid/polymer gel electrolyte, separator modification, or anode surface coating. The high reversibility (99.9% Coulombic efficiency) was found to arise from the formation of a uniform, inorganic SEI made of Na<sub>2</sub>O and NaF, which is highly impermeable to electrolyte solvent and conducive to nondendritic growth. Further efforts are ongoing to investigate the exact mechanism behind the formation of such a uniform, inorganic SEI and will be reported separately. Our proof of concept also shows that the highly reversible Na metal anode can be readily applied in room-temperature Na–S batteries. This work is expected to spur the development of next-generation, Na-based energy storage technologies.

## ■ ASSOCIATED CONTENT

### Supporting Information

The Supporting Information is available free of charge on the ACS Publications website at DOI: 10.1021/acscentsci.5b00328.

Materials and methods and Figures S1–S32 (PDF)

## ■ AUTHOR INFORMATION

## Corresponding Author

\*E-mail: yicui@stanford.edu.

## Present Address

<sup>‡</sup>Z.W.S.: Department of Chemical Engineering, Stanford University, Stanford, California 94305, United States.

## Notes

The authors declare no competing financial interest.

## ■ ACKNOWLEDGMENTS

Y.C. acknowledges the support of the U.S. Department of Energy, Office of Energy Efficiency and Renewable Energy, Battery Materials Research Program. Z.W.S. acknowledges the support of the A\*STAR National Science Scholarship and the help of Dr. Jung Ho Yu in TEM characterization. Part of this work was performed at the Stanford Nano Shared Facilities (SNSF) at Stanford University.

## ■ REFERENCES

- (1) Whittingham, M. S. Electrical energy-storage and intercalation chemistry. *Science* **1976**, *192*, 1126–1127.
- (2) Armand, M.; Tarascon, J.-M. Building better batteries. *Nature* **2008**, *451*, 652–657.
- (3) Goodenough, J. B.; Park, K.-S. The Li-ion rechargeable battery: a perspective. *J. Am. Chem. Soc.* **2013**, *135*, 1167–1176.
- (4) Peled, E. The electrochemical-behavior of alkali and alkaline-earth metals in non-aqueous battery systems - the solid electrolyte interphase model. *J. Electrochem. Soc.* **1979**, *126*, 2047–2051.
- (5) Xu, K. Electrolytes and interphases in Li-ion batteries and beyond. *Chem. Rev.* **2014**, *114*, 11503–11618.
- (6) Verma, P.; Maire, P.; Novak, P. A review of the features and analyses of the solid electrolyte interphase in Li-ion batteries. *Electrochim. Acta* **2010**, *55*, 6332–6341.
- (7) Aurbach, D. Review of selected electrode-solution interactions which determine the performance of Li and Li ion batteries. *J. Power Sources* **2000**, *89*, 206–218.
- (8) Seh, Z. W.; Liu, S.; Han, M.-Y. Titania-coated metal nanostructures. *Chem. - Asian J.* **2012**, *7*, 2174–2184.
- (9) Pan, H.; Hu, Y.-S.; Chen, L. Room-temperature stationary sodium-ion batteries for large-scale electric energy storage. *Energy Environ. Sci.* **2013**, *6*, 2338–2360.
- (10) Slater, M. D.; Kim, D.; Lee, E.; Johnson, C. S. Sodium-ion batteries. *Adv. Funct. Mater.* **2013**, *23*, 947–958.
- (11) Hueso, K. B.; Armand, M.; Rojo, T. High temperature sodium batteries: status, challenges and future trends. *Energy Environ. Sci.* **2013**, *6*, 734–749.
- (12) Yabuuchi, N.; Kubota, K.; Dahbi, M.; Komaba, S. Research development of sodium-ion batteries. *Chem. Rev.* **2014**, *114*, 11636–11682.
- (13) Komaba, S.; Ishikawa, T.; Yabuuchi, N.; Murata, W.; Ito, A.; Ohsawa, Y. Fluorinated ethylene carbonate as electrolyte additive for rechargeable Na batteries. *ACS Appl. Mater. Interfaces* **2011**, *3*, 4165–4168.
- (14) Kim, S.-W.; Seo, D.-H.; Ma, X.; Ceder, G.; Kang, K. Electrode materials for rechargeable sodium-ion batteries: potential alternatives to current lithium-ion batteries. *Adv. Energy Mater.* **2012**, *2*, 710–721.
- (15) Ryu, H.; Kim, T.; Kim, K.; Ahn, J.-H.; Nam, T.; Wang, G.; Ahn, H.-J. Discharge reaction mechanism of room-temperature sodium-sulfur battery with tetra ethylene glycol dimethyl ether liquid electrolyte. *J. Power Sources* **2011**, *196*, S186–S190.
- (16) Hwang, T. H.; Jung, D. S.; Kim, J.-S.; Kim, B. G.; Choi, J. W. One-dimensional carbon-sulfur composite fibers for Na-S rechargeable batteries operating at room temperature. *Nano Lett.* **2013**, *13*, 4532–4538.
- (17) Xin, S.; Yin, Y.-X.; Guo, Y.-G.; Wan, L.-J. A high-energy room-temperature sodium-sulfur battery. *Adv. Mater.* **2014**, *26*, 1261–1265.
- (18) Yu, X.; Manthiram, A. Ambient-temperature sodium-sulfur batteries with a sodiated Nafion membrane and a carbon nanofiber-activated carbon composite electrode. *Adv. Energy Mater.* **2015**, DOI: 10.1002/aenm.201500350.
- (19) Manthiram, A.; Yu, X. Ambient temperature sodium-sulfur batteries. *Small* **2015**, *11*, 2108–2114.
- (20) Liu, W.; Sun, Q.; Yang, Y.; Xie, J.-Y.; Fu, Z.-W. An enhanced electrochemical performance of a sodium-air battery with graphene nanosheets as air electrode catalysts. *Chem. Commun.* **2013**, *49*, 1951–1953.
- (21) Hartmann, P.; Bender, C. L.; Vracar, M.; Duerr, A. K.; Garsuch, A.; Janek, J.; Adelhelm, P. A rechargeable room-temperature sodium superoxide (NaO<sub>2</sub>) battery. *Nat. Mater.* **2013**, *12*, 228–232.
- (22) Xia, C.; Black, R.; Fernandes, R.; Adams, B.; Nazar, L. F. The critical role of phase-transfer catalysis in aprotic sodium oxygen batteries. *Nat. Chem.* **2015**, *7*, 496–501.
- (23) Croce, F.; Appetecchi, G. B.; Persi, L.; Scrosati, B. Nano-composite polymer electrolytes for lithium batteries. *Nature* **1998**, *394*, 456–458.
- (24) Aurbach, D.; Zinigrad, E.; Cohen, Y.; Teller, H. A short review of failure mechanisms of lithium metal and lithiated graphite anodes in liquid electrolyte solutions. *Solid State Ionics* **2002**, *148*, 405–416.
- (25) Monroe, C.; Newman, J. The impact of elastic deformation on deposition kinetics at lithium/polymer interfaces. *J. Electrochem. Soc.* **2005**, *152*, A396–A404.
- (26) Suo, L.; Hu, Y.-S.; Li, H.; Armand, M.; Chen, L. A new class of solvent-in-salt electrolyte for high-energy rechargeable metallic lithium batteries. *Nat. Commun.* **2013**, *4*, 1481.
- (27) Zheng, G.; Lee, S. W.; Liang, Z.; Lee, H.-W.; Yan, K.; Yao, H.; Wang, H.; Li, W.; Chu, S.; Cui, Y. Interconnected hollow carbon nanospheres for stable lithium metal anodes. *Nat. Nanotechnol.* **2014**, *9*, 618–623.
- (28) Park, M. S.; Ma, S. B.; Lee, D. J.; Im, D.; Doo, S.-G.; Yamamoto, O. A highly reversible lithium metal anode. *Sci. Rep.* **2014**, *4*, 3815.
- (29) Xu, W.; Wang, J.; Ding, F.; Chen, X.; Nasybulin, E.; Zhang, Y.; Zhang, J.-G. Lithium metal anodes for rechargeable batteries. *Energy Environ. Sci.* **2014**, *7*, 513–537.
- (30) Qian, J.; Henderson, W. A.; Xu, W.; Bhattacharya, P.; Engelhard, M.; Borodin, O.; Zhang, J.-G. High rate and stable cycling of lithium metal anode. *Nat. Commun.* **2015**, *6*, 6362.
- (31) Lu, Y.; Tu, Z.; Archer, L. A. Stable lithium electrodeposition in liquid and nanoporous solid electrolytes. *Nat. Mater.* **2014**, *13*, 961–969.
- (32) Luo, W.; Zhou, L.; Fu, K.; Yang, Z.; Wan, J.; Manno, M.; Yao, Y.; Zhu, H.; Yang, B.; Hu, L. A thermally conductive separator for stable Li metal anodes. *Nano Lett.* **2015**, *15*, 6149–6154.
- (33) Ryou, M.-H.; Lee, D. J.; Lee, J.-N.; Lee, Y. M.; Park, J.-K.; Choi, J. W. Excellent cycle life of lithium-metal anodes in lithium-ion batteries with mussel-inspired polydopamine-coated separators. *Adv. Energy Mater.* **2012**, *2*, 645–650.
- (34) Kim, J.-S.; Yoo, D.-J.; Min, J.; Shakoob, R. A.; Kahraman, R.; Choi, J. W. Poreless separator and electrolyte additive for lithium-sulfur batteries with high areal energy densities. *ChemNanoMat* **2015**, *1*, 240–245.
- (35) Riechel, T. L.; Wilkes, J. S. Reversible plating and stripping of sodium at inert electrodes in room-temperature chloroaluminate molten-salts. *J. Electrochem. Soc.* **1992**, *139*, 977–981.
- (36) Fuller, J.; Osteryoung, R. A.; Carlin, R. T. Rechargeable lithium and sodium anodes in chloroaluminate molten-salts containing thionyl chloride. *J. Electrochem. Soc.* **1995**, *142*, 3632–3636.
- (37) Gray, G. E.; Kohl, P. A.; Winnick, J. Stability of sodium electrodeposited from a room-temperature chloroaluminate molten-salt. *J. Electrochem. Soc.* **1995**, *142*, 3636–3642.
- (38) Piersma, B. J.; Ryan, D. M.; Schumacher, E. R.; Riechel, T. L. Electrodeposition and stripping of lithium and sodium on inert electrodes in room temperature chloroaluminate molten salts. *J. Electrochem. Soc.* **1996**, *143*, 908–913.
- (39) Park, S. H.; Winnick, J.; Kohl, P. A. Stability of sodium couple in organic and inorganic molten salt electrolytes investigated with

electrochemical quartz crystal microbalance. *J. Electrochem. Soc.* **2001**, *148*, A346–A350.

(40) Wibowo, R.; Aldous, L.; Rogers, E. I.; Ward Jones, S. E.; Compton, R. G. A study of the Na/Na<sup>+</sup> redox couple in some room temperature ionic liquids. *J. Phys. Chem. C* **2010**, *114*, 3618–3626.

(41) Ponrouch, A.; Marchante, E.; Courty, M.; Tarascon, J.-M.; Palacin, M. R. In search of an optimized electrolyte for Na-ion batteries. *Energy Environ. Sci.* **2012**, *5*, 8572–8583.

(42) Bhide, A.; Hofmann, J.; Duerr, A. K.; Janek, J.; Adelhelm, P. Electrochemical stability of non-aqueous electrolytes for sodium-ion batteries and their compatibility with Na<sub>0.7</sub>CoO<sub>2</sub>. *Phys. Chem. Chem. Phys.* **2014**, *16*, 1987–1998.

(43) Jache, B.; Adelhelm, P. Use of graphite as a highly reversible electrode with superior cycle life for sodium-ion batteries by making use of co-intercalation phenomena. *Angew. Chem., Int. Ed.* **2014**, *53*, 10169–10173.

(44) Li, W.; Liang, Z.; Lu, Z.; Yao, H.; Seh, Z. W.; Yan, K.; Zheng, G.; Cui, Y. A sulfur cathode with pomegranate-like cluster structure. *Adv. Energy Mater.* **2015**, *5*, 1500211.

(45) Seh, Z. W.; Yu, J. H.; Li, W.; Hsu, P.-C.; Wang, H.; Sun, Y.; Yao, H.; Zhang, Q.; Cui, Y. Two-dimensional layered transition metal disulphides for effective encapsulation of high-capacity lithium sulphide cathodes. *Nat. Commun.* **2014**, *5*, 5017.

(46) Seh, Z. W.; Wang, H.; Liu, N.; Zheng, G.; Li, W.; Yao, H.; Cui, Y. High-capacity Li<sub>2</sub>S-graphene oxide composite cathodes with stable cycling performance. *Chem. Sci.* **2014**, *5*, 1396–1400.

(47) Sun, Y.; Seh, Z. W.; Li, W.; Yao, H.; Zheng, G.; Cui, Y. In-operando optical imaging of temporal and spatial distribution of polysulfides in lithium-sulfur batteries. *Nano Energy* **2015**, *11*, 579–586.

(48) Zhang, Q.; Wang, Y.; Seh, Z. W.; Fu, Z.; Zhang, R.; Cui, Y. Understanding the anchoring effect of two-dimensional layered materials for lithium-sulfur batteries. *Nano Lett.* **2015**, *15*, 3780–3786.